Cyclotron-resonance maser in a periodically loaded quadrupole transmission line

Y. Leibovitch and E. Jerby*
Faculty of Engineering, Tel Aviv University, Ramat Aviv 69978, Israel
(Received 25 November 1997; revised manuscript received 17 February 1999)

A cyclotron-resonance maser (CRM) is implemented in a periodic quadrupole waveguide. The device oscillates at the fundamental and high harmonics of the cyclotron frequency. This CRM employs a tenuous low-energy electron beam (~10 keV, 0.2 A). The periodic structure consists of an array of disks along the quadrupole transmission line, hence it combines both azimuthal and axial periodicities. This waveguide responds as a band-pass filter (BPF) with uniformly spaced passbands. The CRM is tuned to operate when the cyclotron harmonic frequencies coincide with the waveguide passbands. Microwave emission is observed at the first passband (~2.4 GHz), and simultaneously at the second and third harmonics in the corresponding BPF passbands (~4.9 and ~7.4 GHz, respectively). A polarized detector reveals the circular polarization of the em wave inside the tube. The results of this experiment may lead to the development of novel CRM harmonic generators and CRM arrays. [S1063-651X(99)13108-8]

PACS number(s): 41.60.−m, 84.40.Ik, 84.47.+w

I. INTRODUCTION

Cyclotron-resonance masers (CRMs) and gyrotrons are known as high-power sources of microwaves and millimeter waves [1,2]. In a typical CRM device, an electron beam propagates in a uniform waveguide, immersed in an axial magnetic field. In resonance, the cyclotron motion couples the gyrating electrons to the em wave. The consequent energy transfer, from the electrons to the em wave, causes the CRM amplification.

The CRM interaction at high harmonics of the cyclotron frequency has been a subject of a considerable scientific interest [3–13]. The technological development of high-harmonic CRMs is motivated by practical limitations of available magnets (either permanent or pulsed). The CRM interaction with high harmonics reduces the required magnetic field for a given em frequency, and consequently, decreases the size and weight of the CRM system. High-harmonic gyrotron devices have reached submillimeter wavelengths [13].

CRMs and their derivatives [gyrotrons, cyclotron autoresonance masers (CARMs), etc.] are known as fast-wave devices [14–17]. However, various schemes of slow-wave CRMs have been studied as well [18–27]. The distinction between fast-wave and slow-wave CRM interactions is determined by $V_{\rm ph}>c$ and $V_{\rm ph}<c$, respectively (where $V_{\rm ph}$ is the phase-velocity of the interacting em wave, and c is the speed of light). The slow-wave CRM may operate in an anomalous-Doppler regime [28–32] if $V_{\rm ph}<V_{ez}$ (where V_{ez} is the electron axial velocity). Different CRM mechanisms dominate in the various operating regimes. Hence, slow-wave and fast-wave CRMs differ in their practical implementations and features.

Periodic-waveguide CRMs, studied in amplifier and oscillator schemes [33,34], combine features of both fast-wave and slow-wave CRM interactions. Linear models [35,36] show the feasibility of interactions in various domains. The multibeam CRM-array concept [37] proposes a compact-size, low-voltage and high-power microwave radiator, with active phased-array-antenna features. Theoretical and experimental studies of two-dimensional CRM arrays are in progress [38,39].

Two types of high harmonics are possible in the periodic-waveguide CRM. One is the *spatial* harmonic of the periodic waveguide. The other is the *temporal* harmonic of the cyclotron frequency. Both are included in the CRM tuning relation

$$\omega = n\omega_c \pm V_{ez}\beta_m(\omega), \tag{1}$$

where n is the temporal harmonic order, ω_c is the electron cyclotron frequency, and β_m is the axial wave number of the mth spatial harmonic. The $\pm$ signs denote interactions with forward (+) and backward (−) spatial harmonics. The periodic-waveguide dispersion relation $\beta_m(\omega)$ defines pass bands and stop bands in the frequency domain. The CRM interaction may occur in the fundamental or a higher frequency passband.

In contrast to the CRM interaction in the highly dispersive periodic waveguide, the interaction with a TEM mode in a nondispersive waveguide ($V_{\rm ph}=c$) tends to be weak, unless the initial transverse velocity of the electrons is considerably larger than the axial velocity (i.e., $V_{e\perp} \gg V_{ez}$). On the other

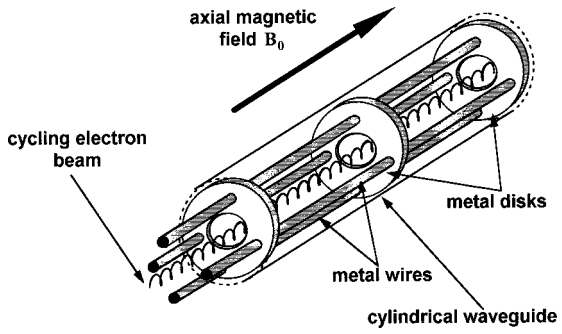

FIG. 1. A section of the quadrupole coupled-cavity CRM structure.

*Author to whom correspondence should be addressed. FAX: +972 3 6423508. Electronic address: jerby@eng.tau.ac.il

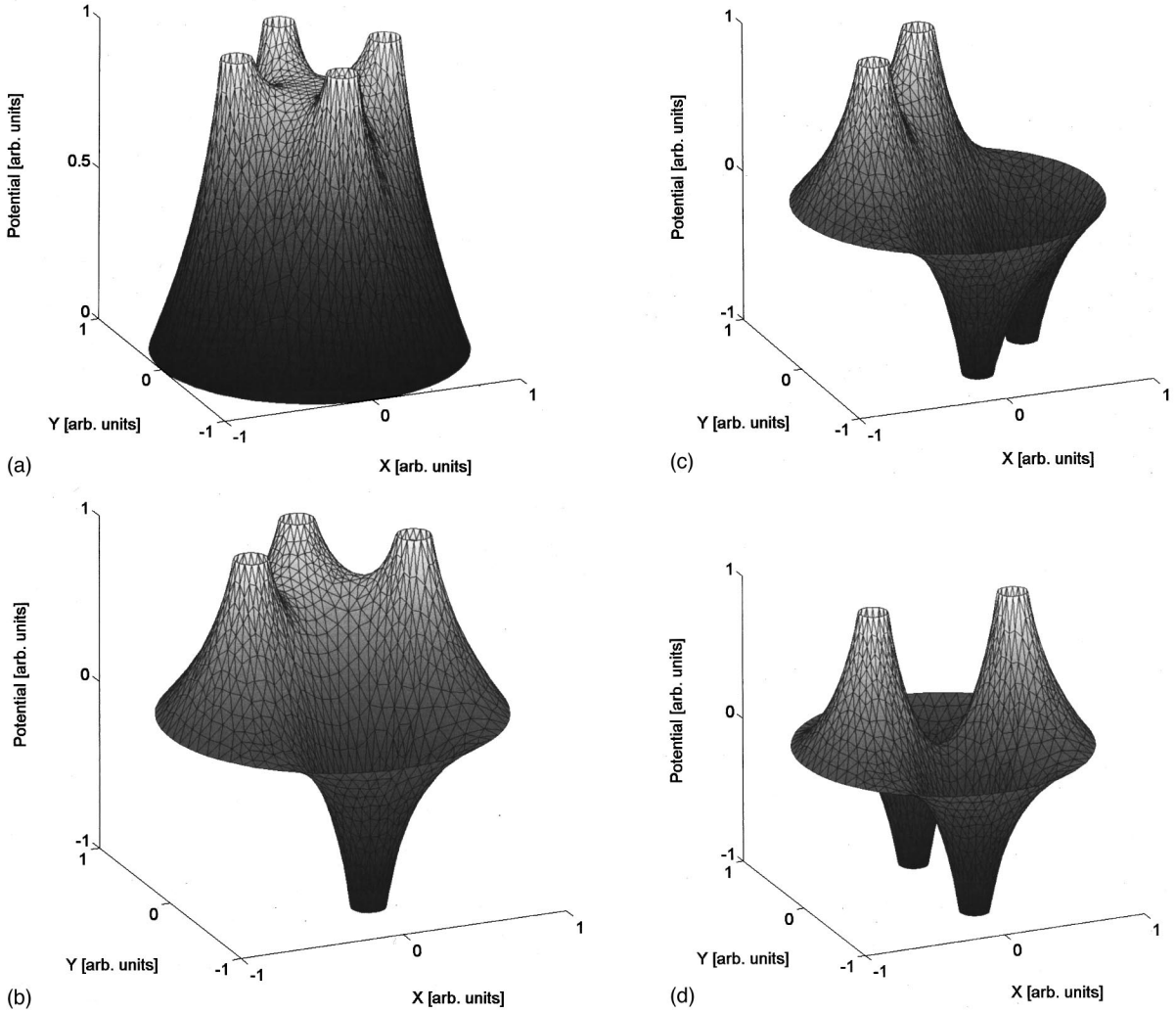

FIG. 2. TEM modes of a uniform quadrupole transmission line without disks. The potential functions result from $\nabla_{\perp}^{2}\Phi=0$.

hand, the tunability range of this device is wide. A recent TEM-CRM experiment demonstrates a tunability range of 1–8 GHz [40].

This paper describes a table-top CRM experiment in a periodic waveguide which consists of a quadrupole transmission line with an array of disks along it. This structure combines azimuthal and axial periodicities. Consequently, it supports CRM interactions with *both* temporal and spatial harmonics in a wide frequency band. The following sections describe the periodic quadrupole waveguide, the CRM experimental setup, and its results.

II. THE PERIODIC QUADRAPOLE STRUCTURE

Figure 1 shows a short section along the coupled-cavity CRM device. The electron beam propagates along the tube while rotating in a cyclotron motion due to the static magnetic field. The periodic waveguide consists of an array of disks along a quadrupole transmission line. The metallic structure in this experiment is made of eight disks and four wires in a cylindrical waveguide. The azimuthal periodicity enables a CRM interaction with high *temporal* harmonics of

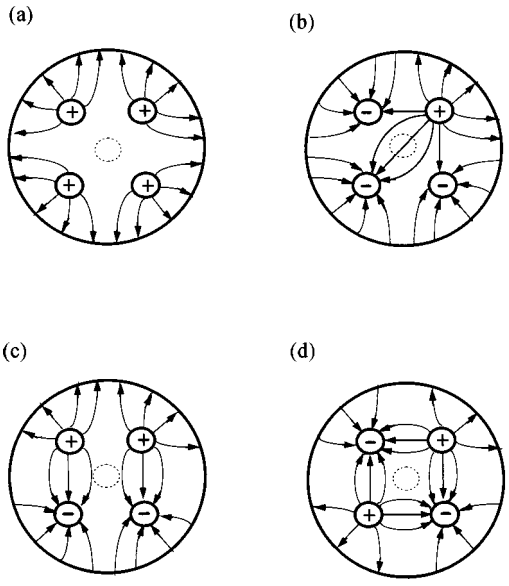

FIG. 3. Schematic TEM-mode field lines corresponding to the potentials in Figs. 2(a)–2(d).

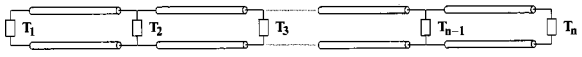

FIG. 4. An equivalent periodic-loaded transmission line. The disks are presented by the reactive elements T_i. The waveguide is terminated by similar elements at both ends.

the cyclotron frequency, whereas the array of disks introduces a longitudinal periodicity and consequently *spatial* harmonics and slow waves.

The quadrupole structure without the disks is a nondispersive waveguide, which supports TEM modes. These can be found by the two-dimensional (2D) Laplace equation $\nabla_\perp^2\Phi=0$, where $\Phi(x,y)$ is the potential function for the electric field, $E_\perp=-\nabla_\perp\Phi$. Both, Φ and $E_\perp$ are illustrated in Figs. 2 and 3, respectively, for the four TEM-mode types supported by the quadrupole transmission line. These TEM modes are characterized by $V_{\rm ph}=c$, $k_z=k_0=\omega/c$, and an impedance $Z=Z_0=120\pi$. The mode shown in Fig. 2(c) is both nonzero on axis and symmetrically balanced, and therefore is most likely to interact with the symmetrical pencil electron beam on axis [note that the mode shown in Fig. 2(b) is also nonzero on axis, but is asymmetrically profiled].

The inclusion of the disks into the quadrupole structure adds periodic reactive elements to the uniform transmission-line, as shown in the equivalent scheme in Fig. 4. The dispersion characteristics of such a periodic transmission-line are described approximately by the general relation [41]

$$\cos(\beta_0 d)=\cos(k_z d)-\frac{1}{2}X\sin(k_z d), \tag{2}$$

where β_0 is the fundamental harmonic wave number of the loaded waveguide, d is the periodic distance between the disks, and X is the normalized reactance introduced by each single disk to the quadrupole waveguide impedance. The wave number of the mth harmonic is $\beta_m=\beta_0+2\pi m/d$, accordingly. The physical dimensions of the experimental waveguide are presented in Fig. 5. As a complementary view to the infinite-periodicity model presented by Eq. (2), the finite periodic waveguide can be regarded as a coupled-cavity structure. Hence, the period d is chosen to be a half wavelength of the desired center frequency 2.45 GHz.

The periodic-waveguide transmission $|S_{21}|$ was measured by a vector network analyzer (HP8510C). Figure 6 shows the spectrum of the first three passbands of the periodic waveguide, equally spaced by a ~2.5 GHz between their center frequencies. In this measurement, the input and output ports were obtained by a small dipole antenna at the entrance to the waveguide, and by a small probe at its exit. No other

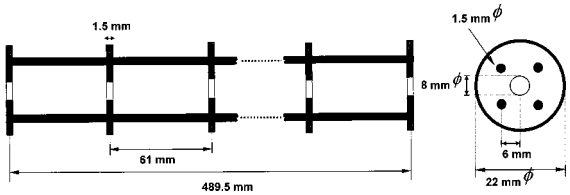

FIG. 5. A mechanical drawing of the periodic structure and its physical dimensions.

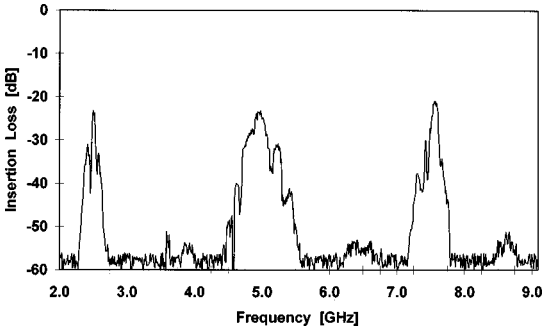

FIG. 6. The transmission $|S_{21}|$ of the periodic waveguide measured by a network analyzer.

passbands were found in different positions or orientations of the input dipole antenna (the only changes were observed in the insertion-loss level within the passbands, where Fig. 6 presents the optimal result). The measured transmission trace combined with Eq. (2) enable the construction of the approximated Brillouin diagram shown in Fig. 7.

A more elaborate analysis of the periodic quadrupole waveguide requires an analysis of Bloch waves as in Ref. [38]. The transverse modes of the periodic waveguide (defined in the middle of each unit cell) resemble those of the uniform waveguide, but their axial wave numbers are expanded to infinite spatial harmonics ($\beta_m=\beta_0+2\pi m/d$). This theoretical problem is intended for a future study. As compared to the known CRM harmonic operation in circularly symmetric devices, the periodic quadrupole imparts an azimuthal transverse variation to the em field seen by the cycling electrons. This transverse modulation is enhanced by the longitudinal periodicity in this device. The TEM-type mode makes the passband equally spaced, and therefore coincide with the CRM harmonics.

III. EXPERIMENTAL SETUP

An overall view of the experimental CRM device is shown schematically in Fig. 8. The device employs a planar electron gun with a thermionic cathode. A solenoid induces the magnetic field profile needed for the CRM interaction (1–3 kG on axis). This device does not employ a separate kicker coil. Synchronized pulsers feed the electron gun and

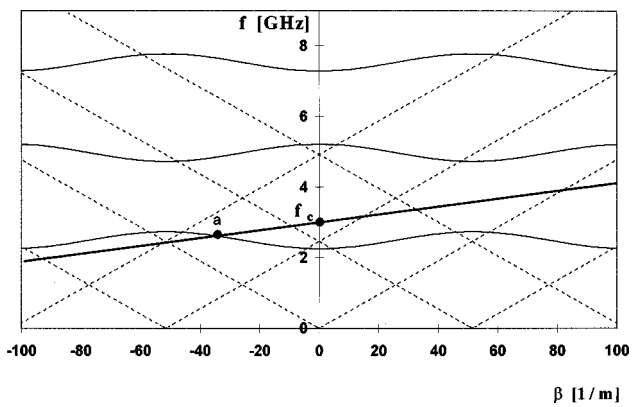

FIG. 7. The Brillouin diagram for the periodic-loaded quadrupole transmission line, and the electron-beam line [Eq. (1)].

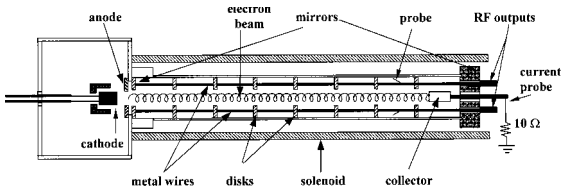

FIG. 8. The experimental CRM device.

the solenoid, as described in Ref. [34]. The electron-gun pulse has a peak voltage of ~10 kV and a pulse width of ~1 ms. The beam current is ~0.2 A and its diameter is 4 mm. Two partial mirrors are placed at both ends of the waveguide. The waveguide is terminated by a collector section connected to the ground by a 10 Ω resistor which enables the electron beam current measurement. The experimental parameters are listed in Table I.

The rf diagnostic setup shown schematically in Figs. 9(a)–9(c) is used to measure the spectral contents of the CRM signal and to detect its polarization. The rf signal is coupled out from the CRM device by small probes attached to each metallic conductor at the end of the quadrupole periodic waveguide. The probes are located in the middle of the last unit cell as shown in Fig. 9(a). In this (fixed) position they are coupled to the maximum electric-field in their vicinity. The four rf probes are identical and symmetrical, and each couples out ~−25 dB of the power in the waveguide. In most runs in this experiment the signal was measured by a single probe, while all others were matched to dummy loads.

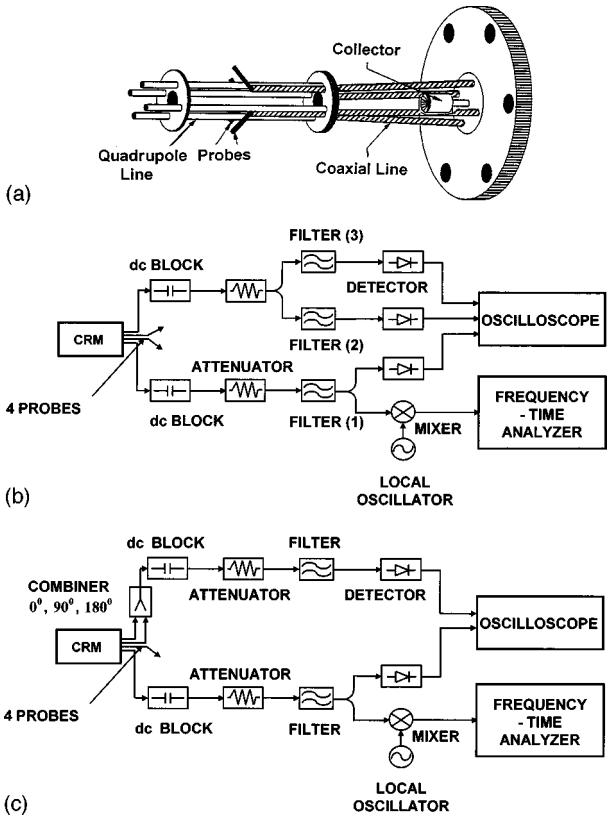

FIG. 9. The microwave diagnostic setup. (a) The rf probe arrangement. (b) The spectral diagnostic. (c) The polarization detector.

TABLE I. Experimental parameters.

Electron energy	~10 keV
Electron current	0.2 A
Pulse width	1 ms
Axial magnetic field	1-3 kG
Interaction length	50 cm
Waveguide period	6.1 cm
Fundamental frequency	2.4 GHz
Output coupled power	~30 W

The spectral analysis setup is shown in Fig. 9(b). The rf output is attenuated by 20 dB attenuators, and divided into various channels. One is terminated by a power detector, and the other by a frequency-time domain analyzer (HP5372A) combined with a mixer (HP5364A) and a synthesized local oscillator (HP83752A). This setup measures the rf variation during the pulse. In addition, the rf sample is filtered by three different band-pass filters (BPFs), each covers a different harmonic of the cyclotron frequency. For the polarization detection, two of the rf-probe outputs are combined in 0°, 90°, and 180° phases by various rf combiners, as shown in

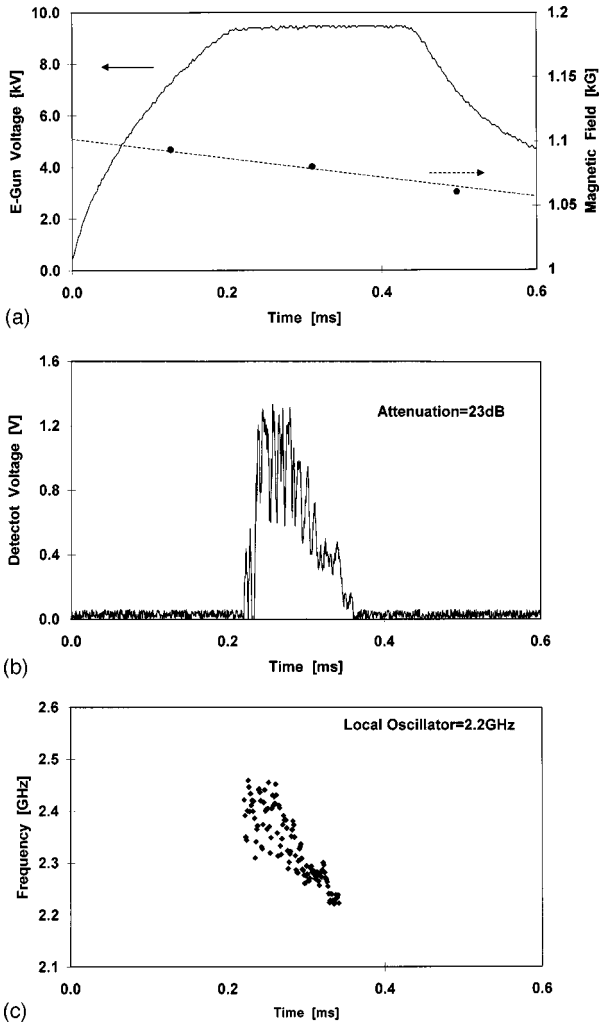

FIG. 10. Typical pulse measurements. (a) The *e*-gun voltage and the magnetic field. (b) The detected rf signal. (c) Its frequency variation during the pulse.

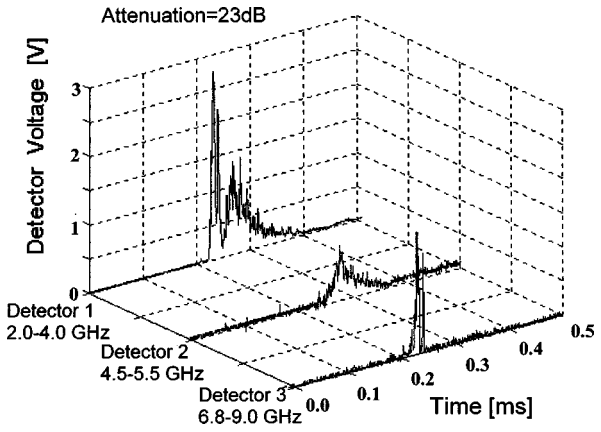

FIG. 11. Simultaneous emission of the first three harmonics in a single pulse.

Fig. 9(c). The third probe provides amplitude and frequency references for the polarization detection.

IV. EXPERIMENTAL RESULTS

The CRM experiment operates in a single pulse, as presented for instance in Figs. 10(a)–10(c). The pulse shape of the electron-gun voltage is shown in Fig. 10(a) with the magnetic-field samples during the pulse. The corresponding collector current is ~0.2 A. Figure 10(b) shows the detected microwave output through a 23 dB attenuator and a BPF (2–4 GHz). The instantaneous frequency measurements during the pulse are shown in Fig. 10(c). The CRM output frequency sweeps from ~2.4 to ~2.2 GHz during the pulse. The axial magnetic field in this run is $B_0 \cong 1.08$ kG, thus the corresponding cyclotron frequency $f_c \cong 3$ GHz is higher than the measured microwave frequency. The Doppler down shift (0.55–0.78 GHz) indicates a CRM interaction with a backward spatial harmonic, as shown figuratively in Fig. 7. The frequency variation during the pulse is attributed by Eq. (1) to the slight variations in the magnetic-field and in the electron energy shown in Fig. 10(a). These variations can be reduced in future experiments by using stabilized pulsers, permanent magnets, etc. It should be noted however that the present experimental limitations provide a ''natural'' sweep which reveals a fundamental CRM tuning effect (1).

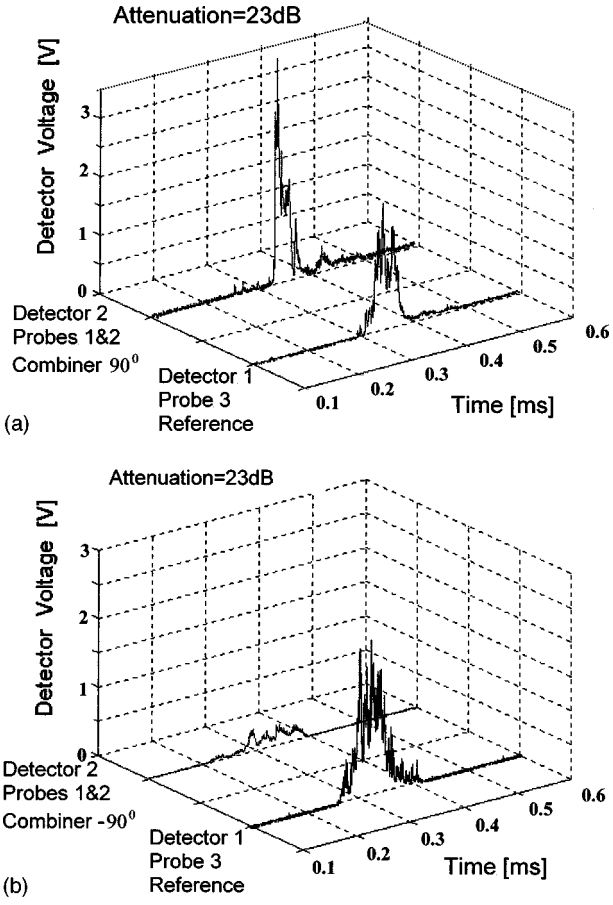

FIG. 12. Polarization detection by summations of two rf-probe outputs in 90° (a) and in −90° (b) phase shifts.

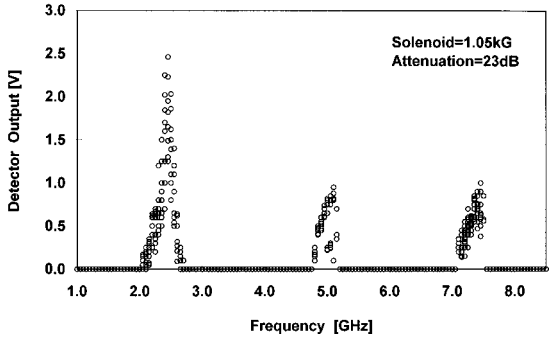

FIG. 13. The harmonic content of the CRM output in the fundamental magnetic field.

The harmonic content of the CRM output signal is detected simultaneously through three high-quality band-pass filters (>40 dB rejection ratio each). The results are shown in Fig. 11. The fundamental harmonic frequency (~2.4 GHz) is detected through a 2.0–4.0 GHz band-pass filter. The next two higher harmonics (at ~4.9 and ~7.4 GHz) are detected through 4.5–5.5 GHz and 6.8–9.0 GHz filters, respectively.

The polarization detection was conducted by the setup shown in Fig. 10(c). The outputs of the microwave combiner (fed by two different probes) are shown in Figs. 12(a) and 12(b). The combination of two adjacent probes through a 90° combiner is shown in Fig. 12(a). This sum of the two signals yields almost twice larger amplitude than the reference signal measured by the third probe. In other runs, the output signals of two distant probes are combined by a −90° com-

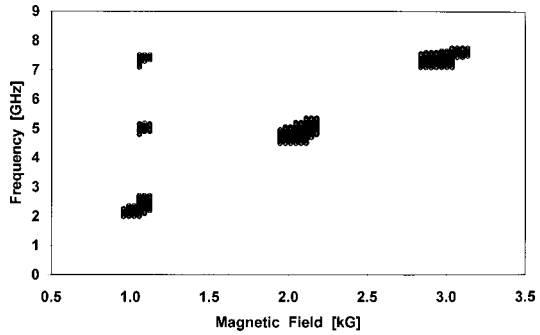

FIG. 14. The spectral content of the CRM output vs the magnetic field.

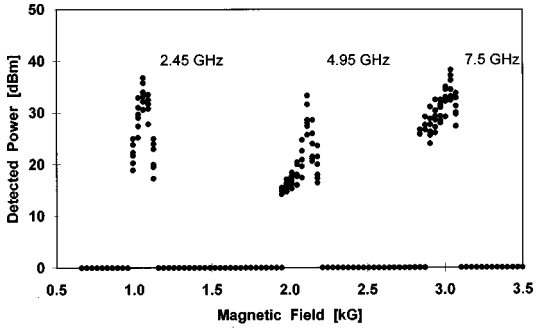

FIG. 15. The detector output vs the magnetic field.

biner. The resulting signal is substantially smaller than the reference signal, as shown in Fig. 12(b). This indicates that the fields near the two distant conductors are in opposite phases. The results presented in Figs. 12(a) and 12(b) show that a *circular* polarization is evolved by the CRM interaction inside the quadrupole coupled-cavity structure. This finding has been confirmed by many similar measurements conducted with all possible combinations of adjacent or distant probes. These results show, conclusively, a phase difference of 90° between two adjacent probes. For TEM modes, this feature indicates a circular polarization (note that in the given waveguide dimensions and frequency range, all other modes except TEM are in cutoff).

Figure 13 shows the spectral content of the CRM emission. The measurements were accumulated in many runs in the same conditions through three band-pass filters (2.0–4.0 GHz, 4.5–5.5 GHz, and 6.8–9.0 GHz). The results show clearly three harmonics around the center frequencies ~2.4, ~4.9, and ~7.4 GHz. The fundamental harmonic signal is larger by 6–8 dB than the second or the third harmonics.

Figure 14 shows the spectral content of the CRM output versus the solenoid axial magnetic field. Three frequency bands are observed simultaneously at a magnetic field of ~1 kG. Increasing the magnetic field to ~2 or ~3 kG results in microwave emissions in the second or third passband frequencies, around ~5 or ~7 GHz, respectively. Figure 15 shows the output power of the microwave emission in the fundamental frequency in different magnetic fields, as measured by a single probe (while the others are terminated by matched loads). An rf power of over 30 W is coupled out by the probes at the first or third harmonic frequencies.

Figures 16(a) and 16(b) show the spectral contents of the CRM output at the fundamental harmonic in the second and third passband frequencies, at 2.15 and 3.1 kG magnetic fields, respectively. The results shown in Figs. 13–16, accumulated in many runs, form a spectrum which coincides with the (cold) waveguide transmission measurement shown in Fig. 6.

V. CONCLUSIONS

The experimental results presented in this paper show the feasibility of a CRM device in a periodic quadrupole (coupled-cavity) structure. rf oscillations are observed near the cyclotron frequency and its second and third harmonics. The device is tunable in a wide frequency range by varying the axial magnetic field (and consequently the cyclotron frequency) to match the periodic-waveguide passband.

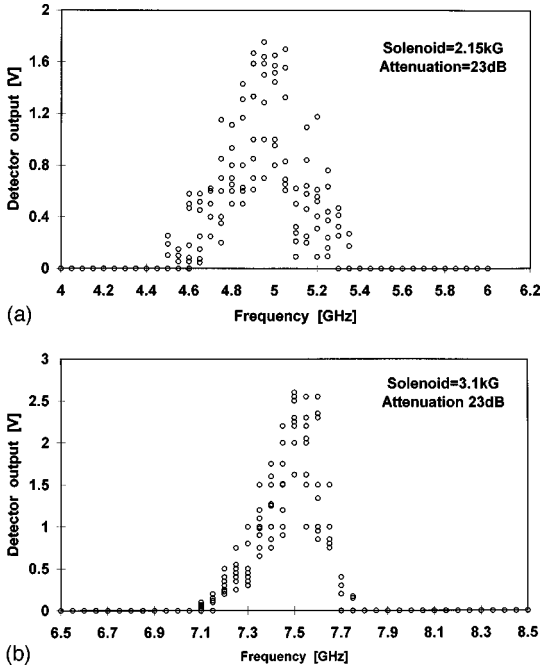

FIG. 16. Spectral contents of the CRM output at the second (a) and the third (b) magnetic-field levels.

The experimental waveguide combines a nondispersive quadrupole transmission line with a periodic array of disks along it. It merges features of CRM interactions with TEM modes, and with spatial harmonics and Bloch waves. The quadrupole line enables the wave propagation below the cutoff of the outer cylindrical waveguide. In addition to the *dipole* wave profile [Fig. 3(c)] [40], it supports also a *quadrupole* TEM mode [Fig. 3(d)] which may enable a high-harmonic cyclotron interaction with large-orbit electrons.

The CRM interaction in this experimental scheme does not require a strong kicker to impart a transverse velocity component to the electrons. This alleviation is typical to periodic waveguide CRMs, in particular at the anomalous Doppler regime, and it has a considerable practical advantage (note that the large kicker required to amplify pure TEM modes impedes their applicability in practical CRM devices).

The experimental results show that the em wave excited by the CRM interaction in the quadrupole waveguide is circularly polarized. This feature strengthens the CRM interaction as compared to the linearly polarized devices presented in Refs. [34,40].

Further studies of the quadrupole-CRM scheme are needed toward the development of a useful device. For practical applications, an efficient output coupler to the quadrupole line should be developed. The simultaneous emission in harmonic frequencies observed in this experiment could be beneficial for applications, such as ceramic sintering [42]. The quadrupole CRM can be regarded as a step toward CRMs with higher-order transmission lines of six, eight, and even more parallel wires. These structures resemble *photonic-bandgap* waveguides which could be investigated in this context [43]. Another exciting scheme promoted by the present experiment is the conceptual CRM array, which could be implemented by quadrupole-CRM elements in a covalent lattice [37].

[1] J. Benford and J. Swegle, *High-Power Microwaves* (Artech House, Boston, 1992).
[2] *High-Power Microwave Sources*, edited by V. L. Granatstein and I. Alexeff (Artech House, Boston, 1987).
[3] D. V. Kisel, G. S. Korablev, V. G. Pavel'yev, M. I. Petelin, and Sh. Ye. Tsimring, Radio Eng. Electron. Phys. **19**, 95 (1974).
[4] C. M. Tang, S. Riyopoulos, P. Sprangle, and B. Levush, Nucl. Instrum. Methods Phys. Res. A **252**, 192 (1987).
[5] D. S. Furuno, D. B. McDermott, H. Cao, C. S. Kou, N. C. Luhmann, Jr., P. Vitello, and K. Ko, Int. J. Electron. **65**, 429 (1988).
[6] T. Idehara, T. Tatsukawa, S. Matsumoto, K. Kunieda, K. Hemmi, and T. Kanemaki, Phys. Lett. A **132**, 344 (1988).
[7] S. Spira-Hakkarainen, K. E. Kreischner, and R. J. Temkin, IEEE Trans. Plasma Sci. **18**, 334 (1990).
[8] C. S. Kou, D. B. McDermott, N. C. Luhmann, Jr., and K. R. Chu, IEEE Trans. Plasma Sci. **18**, 343 (1990).
[9] G. F. Brand, P. W. Fekete, K. Hong, K. J. Moore, and T. Idehara, Int. J. Electron. **68**, 1099 (1990).
[10] G. S. Nusinovich and Nai Li, IEEE Trans. Plasma Sci. **20**, 170 (1992).
[11] D. Wagner, G. Gantenbein, W. Kasparek, and M. Thumm, Int. J. Infrared Millim. Waves **16**, 1481 (1996).
[12] V. Bratman (unpublished).
[13] Y. Shimizo, S. Makino, K. Ichikawa, T. Tatsukawa, T. Idehara, and I. Ogawa, Phys. Plasmas **2**, 2110 (1996).
[14] N. I. Zaytsev, T. V. Pankratova, M. I. Petelin, and V. A. Flyagin, Radio Eng. Electron. Phys. **19**, 103 (1974).
[15] S. Y. Park, R. H. Kyser, C. M. Armstrong, R. K. Parker, and V. L. Granatstein, IEEE Trans. Plasma Sci. **18**, 321 (1990).
[16] N. A. Nikolov, I. P. Spasovsky, K. G. Kostov, J. N. Velichkov, V. A. Spasov, and I. G. Yovchev, J. Appl. Phys. **67**, 7620 (1990).
[17] A. C. DiRienzo, G. Bekefi, C. Chen, and J. S. Wurtele, Phys. Fluids B **3**, 1755 (1991).
[18] K. R. Chu, P. Sprangle, and V. L. Granatstein, Bull. Am. Phys. Soc. **23**, 748 (1978).
[19] K. R. Chu, A. K. Ganguly, V. L. Granatstein, J. L. Hirshfield, S. Y. Park, and J. M. Baird, Int. J. Electron. **51**, 493 (1981).
[20] H. Guo, L. Chen, H. Keren, and J. L. Hirshfield, Phys. Rev. Lett. **49**, 730 (1982).
[21] H. S. Uhm and J. Y. Choe, Phys. Fluids **26**, 3418 (1983).
[22] N. T. Cherpak and T. A. Smirnova, Sov. J. Commun. Technol. Electron. **30**, 74 (1985).
[23] T. H. Kho and A. T. Lin, Phys. Rev. A **38**, 2883 (1988).
[24] D. B. McDermott, H. B. Cao, and N. C. Luhmann, Int. J. Electron. **65**, 477 (1988).
[25] A. K. Ganguly and S. Ahn, Phys. Rev. A **42**, 3544 (1990).
[26] K. C. Leou, D. B. McDermott, and N. C. Luhmann, Jr., IEEE Trans. Plasma Sci. **20**, 188 (1992).
[27] K. Minami (private communication).
[28] B. I. Ivanov, D. V. Gorozhanin, and V. A. Miroshnichenko, Sov. Tech. Phys. Lett. **5**, 464 (1979).
[29] S. Yu. Galuzo, V. I. Kanavets, A. I. Slepkov, and V. A. Pletyushkin, Sov. Tech. Phys. Lett. **27**, 1030 (1982).
[30] A. N. Didenko, A. R. Borisov, G. P. Fomenko, A. S. Shlapakovskii, and Yu. G. Shtein, Sov. Tech. Phys. Lett. **9**, 572 (1983).
[31] A. V. Korzhenevskii and V. A. Cherepenin, Sov. Phys. Tech. Phys. **34**, 1254 (1989).
[32] M. Einat and E. Jerby, Phys. Rev. E **56**, 5996 (1997).
[33] E. Jerby and G. Bekefi, Phys. Rev. E **48**, 4637 (1993).
[34] E. Jerby, A. Shahadi, V. Grinberg, V. Dikhtiar, M. Sheinin, E. Agmon, H. Golombek, V. Trebich, M. Bensal, and G. Bekefi, IEEE J. Quantum Electron. **31**, 970 (1995).
[35] E. Jerby, Phys. Rev. E **49**, 4487 (1994).
[36] M. Korol and E. Jerby, Nucl. Instrum. Methods Phys. Res. A **375**, 222 (1996).
[37] E. Jerby, A. Kesar, Li Lei, M. Korol, and V. Dikhtyar, IEEE Trans. Plasma Sci. **27**, 445 (1999).
[38] M. Korol and E. Jerby, Phys. Rev. E **55**, 5934 (1997).
[39] Li Lei and E. Jerby, Phys. Rev. E **59**, 2322 (1999).
[40] E. Jerby, A. Shahadi, R. Drori, M. Korol, M. Einat, I. Ruvinsky, M. Sheinin, V. Dikhtiar, V. Grinberg, M. Bensal, T. Harhel, Y. Baron, A. Fruchtman, V. L. Granatstein, and G. Bekefi, IEEE Trans. Plasma Sci. **24**, 816 (1996).
[41] R. E. Collin, *Foundations of Microwave Engineering* (McGraw Hill, New York, 1992).
[42] Y. Carmel (private communication).
[43] M. Shapiro (private communication).